doi: 10.5937/SimTerm24333P

Mixed Convective EMHD Flow of a Ternary Hybrid Nanofluid in a Vertical Channel with Porous Medium

Jelena Petrović[a], Milica Nikodijević Đorđević[b], Miloš Kocić[c], Jasmina Bogdanović Jovanović[d], Živojin Stamenković[e]

[a]*Faculty of Mechanical Engineering, Niš, RS, jelena.nikodijevic.petrovic@masfak.ni.ac.rs*
[b]*Faculty of Occupational Safety, Niš, RS, milica.nikodijevic@znrfak.ni.ac.rs,*
[c]*Faculty of Mechanical Engineering, Niš, RS, milos.kocic@masfak.ni.ac.rs*
[d]*Faculty of Mechanical Engineering, Niš, RS, jasmina.bogdanovic.jovanovic@masfak.ni.ac.rs*
[e]*Faculty of Mecanical Engineering, Niš, RS, zivojin.stamenkovic@masfak.ni.ac.rs*

Abstract: This paper considers the mixed convective EMHD flow of a ternary hybrid nanofluid in a vertical channel. There is a homogeneous porous medium in the channel whose walls are on different temperatures. A homogeneous magnetic field acts perpendicular to the channel walls and a homogeneous electric field acts perpendicular to the direction of the fluid flow. The base fluid is blood and nanoparticles of three types of materials are suspended in it. The induced magnetic field is neglected. Velocity and temperature distributions were analytically determined and presented in the form of graphs. The shear stresses and Nusselt numbers on the channel walls are calculated and tabulated.

Keywords: EMHD, Ternary hybrid nanofluid, Vertical channel, Porous medium, Nusselt number.

1. Introduction

Convective heat transport is present in many industrial processes, energy, medicine, etc. Because of his wide presence, his research has become an important topic for researchers of various specialties. A large number of researchers are dedicated to improving heat transport by increasing heat transfer surfaces, vibration of these surfaces, use of microchannels, etc. The low thermal conductivity of classical fluids compared to metals has been observed, and research is being carried out in order to increase it.

Choi [1] suggested improving the thermal conductivity of fluids by suspending nanometer-sized metal particles and called these fluids nanofluids. Today, a lot of researchers are dedicated to nanofluids and hybrid nanofluids. Attention is drawn to the fact that nanofluid heat transport in a magnetic environment is a relatively new research area. The minimal number of studies mentioned in this introduction sufficiently shows how wide their range is.

In the paper by Lima et al. [2], EMHD flow and heat transfer of two immiscible fluids in a channel between two inclined parallel plates were investigated. The effects of layer porosity, buoyancy, Joule and viscous heating, moving plates, tilted magnetic field and heat generation/absorption are included. Raju and Satish [3] investigated the influence of slip factor on EMHD flow and heat transfer of two immiscible plasma fluids in a horizontal channel between two parallel plates with Hall currents. Nikodijevic et al. [4] investigated unsteady magnetohydrodynamic flow and heat transfer in a horizontal channel between parallel plates. The medium in the channel is porous, and the applied magnetic field is inclined relative to the direction of the primary current. The influence of magnetic field and thermal radiation on entropy generation of immiscible micropolar and Newtonian fluid in a horizontal rectangular channel of porous medium was investigated by Yadav et al. [5]. Gul et al. [6] investigated the effects of radiation and heat generation in unsteady MHD mixed convective flow of nanofluids in a vertical channel. The influence of the size of nanoparticles on speed and temperature was analyzed in particular. Das et al. [7] investigated the MHD fully developed mixed convective flow of a nanofluid in a vertical channel. An induced magnetic field is included. Umavathi and Sheremet [8] investigated the mixed convection in a vertical channel where in its middle part there is a Newtonian fluid, and in the end parts, where the media are porous, there are nanofluids. Double-diffusion and forced convective flow of nanofluids in a vertical channel with Robin boundary conditions on the channel walls was investigated by Umavathi and Chamkha [9]. Umavathi and Oztop [10] presented a numerical simulation for the analysis of the influence of electric and magnetic fields on the flow and heat transfer of nanofluids in a vertical channel. Petrovic et al. [11, 12] investigated EMHD flow and heat transfer of immiscible viscous and nanofluids in horizontal and vertical channels, respectively, whose media are porous. The channel walls are impermeable and are at constant but different temperatures. EMHD flow and heat transfer of Casson nanofluid Fe_3O_4- blood in a horizontal channel of a porous medium with isothermal and impermeable walls was investigated by Petrovic et al. [13]. The influence of different nanoparticles on unsteady MHD flow and heat transfer of immiscible viscous and nanofluids in an inclined channel of porous media and permeable walls was investigated by Devi et al. [14]. The influence of the nanoparticle shape factor on the oscillatory MHD flow of two immiscible nanofluids in a horizontal channel of a porous medium with thermal radiation and sliding velocity and temperature on the channel walls was investigated by Devi et al. [15].

Xu and Sun [16] investigated the fully developed convective flow of a generalized hybrid nanofluid in a vertical microchannel. Chamkha et al. [17] investigated the MHD flow and heat transfer of a hybrid nanofluid in a vertical microchannel. Chamkha et al. [18] investigated the MHD flow and heat transfer of a hybrid nanofluid in a rotating system between two parallel plates that are permeable and stretchable under the influence of thermal radiation. Sudharani et al. [19] investigated the flow and heat transfer of a hybrid/trihybrid nanofluid over a moving plate. The influence of slip and radiation is included. It is shown that the rate of heat transfer in three hybrid nanofluids is higher than in hybrid nanofluids. Ebrahem [20] investigated the natural convective flow of three hybrid nanofluids along a horizontal stretchable sheet in a porous medium with radiation and chemical reaction. The main goal of this research is to examine the flow characteristics of this fluid for industrial and biomedical applications. Riaz et al. [21] investigated the MHD flow of non-Newtonian Willianson three hybrid nanofluids in a porous medium over a horizontal stretchable plate with thermal radiation.

By reviewing the existing research, it becomes clear that the simultaneous effects of magnetic field, electric field, viscous, Joule's and Darcy's dissipation on the convective flow of three hybrid nanofluids have not been sufficiently investigated. This especially applies to trihybrid nanofluids whose base fluid is blood. Therefore, in this work, the EMHD convective flow of trihybrid nanofluid Al_2O_3+MgO+TiO_2/blood in a vertical channel whose medium is porous is investigated. Application of the results of this research is expected in many fields, especially in medicine.

2. Mathematical formulation

The problem investigated here is the mixed convective flow of three hybrid nanofluids in a channel between two parallel vertical walls (see Figure 1). The medium in the channel is porous, and its permeability is The walls of the channel are at a mutual distance h, are impermeable and are at constant temperatures on both the right and left sides, respectively. The applied magnetic field of induction B is perpendicular to the walls of the channel, and the applied electric field of strength E is perpendicular to the longitudinal plane of the channel perpendicular to its walls. The pressure gradient in the flow direction is constant, and the flow is laminar, stationary and fully developed.

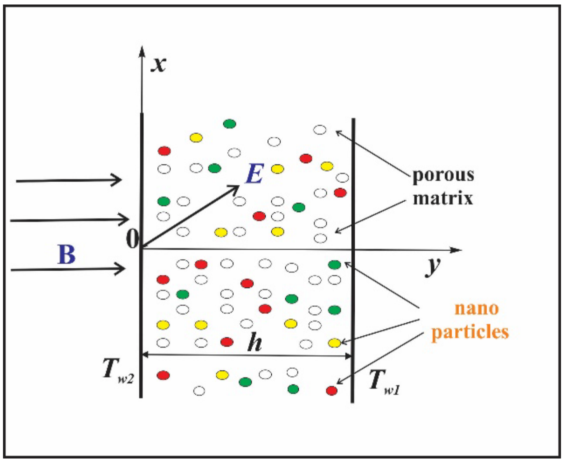

Fig.1 Physical model

The described problem is mathematically formulated by the momentum equation, energy equation and boundary conditions, respectively [8, 12]:

$$-\frac{dp}{dx}+\mu\frac{d^2U}{dZ^2}-\frac{\mu}{K_0}U-B\sigma\left(E+Bu\right)+g\left(\rho\beta\right)\left(T-T_{w2}\right)=0, \tag{23}$$

$$k\frac{d^2T}{dY^2}+\mu\left(\frac{dU}{dY}\right)^2+\frac{\mu}{K_0}U^2+\sigma(E+Bu)^2=0, \tag{2}$$

$$(u,T)(0)=(0,T_{w2}),\ (U,T)(h)=(0,T_{w1}), \tag{3}$$

where the labels are used: $X,Y-$ Cartesian coordinates, $g-$ gravitational acceleration, $p,T,u-$ pressure, velocity, temperatures of the three hybrid nanofluids, respectively, and $\rho,\beta,\mu,k,\sigma-$ the properties of the three hybrid nanofluids are density, coefficient of thermal expansion, coefficient of dynamic viscosity, coefficient of thermal conductivity and electrical conductivity, respectively.

The physical properties of three hybrid nanofluids are given by relations [19]:

$$\begin{aligned}
&\rho=\omega_2\rho_f,\omega_2=(1-\phi_3)\omega_1+\phi_3\frac{\rho_3}{\rho_f},\\
&\omega_1=(1-\phi_2)\omega_0+\phi_2\frac{\rho_2}{\rho_f},\omega_0=1-\phi_1+\phi_1\frac{\rho_1}{\rho_f},\\
&\mu=\frac{\mu_f}{m},\ m=(1-\phi_1)^{2.5}(1-\phi_2)^{2.5}(1-\phi_3)^{2.5},k=\varphi_2k_f,\varphi_2=N(\phi_3,k_3,k_f,\varphi_1),\\
&\varphi_1=N(\phi_2,k_2,k_f,\varphi_0),\ \varphi_0=N(\phi_1,k_1,k_f,1),N(\phi,S,R,M)=\frac{(1+2\phi)S+2(1-\phi)RM}{(1-\phi)S+(2+\phi)RM},\\
&\sigma=\varphi_4\sigma_f,\ \varphi_4=N(\phi_3,\sigma_3,\sigma_f,\varphi_3),\varphi_3=N(\phi_2,\sigma_2,\sigma_f,\varphi_0^*),\ \varphi_0^*=N(\phi_1,\sigma_1,\sigma_f,1)\\
&(\rho\beta)=\varphi_6(\rho\beta)_f,\ \varphi_6=L(\phi_3,\sigma_5,3),\ \varphi_6=L(\phi_2,\sigma_s^*,2),\varphi_5^*=L(\phi_1,1,1),\\
&L(\phi,M,i)=(1-\phi)M+\phi\frac{(\rho\beta)_i}{(\rho\beta)_f},(\rho c_p)=\Psi_2(\rho c_p)_f,\ \Psi_2=D(\phi_3,\Psi_1,3),\Psi_1=D(\phi_2,\Psi_0,2),\\
&\Psi_0=D(\phi_1,1,1),D(\phi,M,i)=(1-\phi)M+\phi\frac{(\rho c_p)_i}{(\rho c_p)_f}.
\end{aligned} \tag{4}$$

where the indices 1, 2 and 3 refer to the material properties and volume fractions of nanoparticles 1, 2 and 3 and the index f refers to the properties of the base fluid.

Introducing further dimensionless transformations:

$$y^*=\frac{Y}{h},u=\frac{U}{U_0},\ \theta=\frac{T-Tw_2}{Tw_1-Tw_2},$$

and the volume fractions ϕ in which there is characteristic velocity U_0 and using relations (3) of equations (1), (2) and boundary conditions (3) are, respectively, transformed to:

$$\frac{d^2u}{dy^2}-\omega^2u+aM\Theta=R_1, \tag{5}$$

$$\frac{d^2\theta}{dy^2}+\frac{Br}{m\varphi_2}\left[\left(\frac{du}{dy}\right)^2+\omega^2u^2+2Ru+R_2\right]=0, \tag{6}$$

$$(u,\theta)(0)=(0,0),\ (u,\theta)(1)=(0,1). \tag{7}$$

where tags are used:

$$\begin{aligned}
&\Lambda=\frac{h^2}{K_0},Ha=Bh\sqrt{\frac{\sigma_f}{\mu_f}},K=\frac{E}{BU_0},M=g\frac{(\rho\beta)_f h(Tw_1-Tw_2)^2}{\mu_fU_0},\\
&P=-\frac{\partial p}{\partial X}\frac{h^2}{U_0\mu_f},\ \omega^2=\Lambda+m\varphi_4Ha^2,a=m\varphi_6,R=m\varphi_4KHa^2,\\
&R_1=R-mP,\Pr=\frac{\mu_fc_{pf}}{k_f},\ Ec=\frac{U_0^2}{c_{pf}(Tw_1-Tw_2)},\\
&Br=\Pr Ec,R_2=RK,
\end{aligned} \tag{8}$$

where are: Λ – porosity factor, Ha – Hartmann number, K – electric load factor, Pr – Prandtl number, Ec – Eckert number, Br – Brinkman number.

3. Solution method

Equations (5) and (6) are non-linear, simultaneous differential equations and it is not possible to analytically find their exact solution. That is why their approximate solution will be analytically determined here, and the perturbation method will be used for that. To that end, the approximate solution can be presented in the form:

$$(u,\theta)(y)=(u_0,\theta_0)(y)+Br(u_1,\theta_1)(y), \tag{9}$$

where the Brinkman number is used as the perturbation parameter.

Using relation (9) and the perturbation method from equations (5), (6) and zero-order boundary conditions:

$$\frac{d^2u_0}{dy^2}-\omega^2u_0+aM\theta_0=R_1, \tag{10}$$

$$\frac{d^2\theta_0}{dy^2}=0, \tag{11}$$

$$(u_0,\theta_0)(0)=(0,0),\ (u_0,\theta_0)(1)=(0,1), \tag{12}$$

and equations and boundary conditions of the first order:

$$\frac{d^2u_1}{dy^2}-\omega^2u_1+aM\theta_1=0, \tag{13}$$

$$\frac{d^2\theta_1}{dy^2}+\frac{1}{m\varphi_2}\left[\left(\frac{du_0}{dy}\right)^2+\omega {u_0}^2+2Ru_0+R_2\right]=0, \tag{14}$$

$$(u_1,\theta_1)(0)=(0,0),\ (u_1,\theta)_1(1)=(0,0). \tag{15}$$

The solution of equations (10) and (11) with boundary conditions (12) is:

$$u_0(y)=D_1\exp(\omega y)+D_2\exp(-\omega y)+\frac{aM}{\omega^2}y-\frac{R_1}{\omega^2}, \tag{16}$$

$$\theta_0(y)=y. \tag{17}$$

The solution of equations (13) and (14) with boundary conditions (15) is:

$$D_1=\frac{R_1[1-\exp(-\omega)]-aM}{\omega^2[\exp(\omega)-\exp(-\omega)]},\ D_2=\frac{R_1}{\omega^2}-D_1. \tag{18}$$

The solution of equations (13) and (14) with boundary conditions (15) is:

$$\begin{aligned}u_1(y)&=D_3\exp(\omega y)+D_4\exp(-\omega y)+R_{10}\exp(2\omega y)+R_{11}\exp(-2\omega y)+\\&y(R_{12}+R_{13}y)\exp(\omega y)+y(R_{14}+R_{15}y)\exp(-\omega y)+\\&R_{16}y^4+R_{17}y^3+R_{18}y^2+R_{19}y+R_{20}\end{aligned} \tag{19}$$

$$\begin{aligned}\theta_1(y)&=-\frac{1}{m\varphi_2}[\frac{1}{2}D_1^2\exp(2\omega y)+\frac{1}{2}D_2^2\exp(-2\omega y)+(R_3+R_4y)\exp(\omega y)+\\&(R_5+R_6y)\exp(-\omega y)+R_7y^4+R_8y^3+R_9y^2+C_3y+C_4],\end{aligned} \tag{20}$$

where tags are used:

$$R_3=\frac{2D_1}{\omega^2}(R-R_1-\frac{aM}{\omega}),R_4=\frac{2MaD_1}{\omega^2},\ R_5=\frac{2D_2}{\omega^2}(R-R_1+\frac{aM}{\omega}),$$
$$R_6=\frac{2MaD_2}{\omega^2},R_7=\frac{a^2M^2}{12\omega^2},\ R_8=\frac{aM}{3\omega^2}(R-R_1),$$
$$R_9=\frac{1}{2}(\frac{a^2M^2}{\omega^4}+\frac{R_1^2}{\omega^2}-\frac{2RR_1}{\omega^2}+R_2),\ S=\frac{aM}{m\varphi_2},$$
$$R_{10}=\frac{SD_1^2}{6\omega^2},\ R_{11}=\frac{SD_2^2}{6\omega^2},\ R_{12}=S\frac{2\omega R_3-R_4}{4\omega^2},$$
$$R_{13}=\frac{SR_4}{4\omega},\ R_{14}=-S\frac{2\omega R_5+R_6}{4\omega^2},\ R_{15}=-S\frac{R_6}{4\omega},$$
$$R_{16}=-S\frac{R_7}{\omega^2},\ R_{17}=-S\frac{R_8}{\omega^2},\ R_{18}=-S\frac{12R_7+\omega^2R_9}{\omega^4},$$
$$R_{19}=-S\frac{6R_8+\omega^2C_3}{\omega^4},\ R_{20}=-S\frac{24R_7+2\omega^2R_9+\omega^4C_4}{\omega^6},$$

$$\begin{aligned}&R_{21}=-R_{10}-R_{11}-R_{20},\ R_{22}=-R_{10}\exp(2\omega)-\\&R_{11}\exp(-2\omega)-(R_{12}+R_{13})\exp(\omega)-(R_{14}+R_{15})\exp(-\omega)\\&-R_{16}-R_{17}-R_{18}-R_{19}-R_{20},\\&C_3=\frac{1}{2}(D_1^2+D_2^2)+R_3+R_5-\frac{1}{2}D_1^2\exp(2\omega)\\&-\frac{1}{2}D_2^2\exp(-2\omega)-(R_3+R_4)\exp(\omega)-\\&(R_5+R_6)\exp(-\omega)-R_7-R_8-R_9,\\&C_4=-\frac{1}{2}(D_1^2+D_2^2)-R_3-R_5,\\&D_3=\frac{R_{22}-R_{21}\exp(-\omega)}{\exp(\omega)-\exp(-\omega)},\ D_4=R_{21}-D_3.\end{aligned} \tag{21}$$

Thus, the velocity and temperature distributions of three hybrid nanofluids in the problem considered here are determined.

The dimensionless shear stresses on the left and right channel walls are given, respectively, by the relations:

$$\begin{aligned}\tau_1&=\frac{\mu}{\mu_f}\left(\frac{du}{dy}\right)_{y=0},\\ \tau_2&=\frac{\mu}{\mu_f}\left(\frac{du}{dy}\right)_{y=1},\end{aligned} \tag{22}$$

and the Nusselt numbers on these walls, respectively, are:

$$\begin{aligned}Nu_1&=\frac{k}{k_f}\left(\frac{d\theta}{dy}\right)_{y=0},\\ Nu_2&=\frac{k}{k_f}\left(\frac{d\theta}{dy}\right)_{y=1}.\end{aligned} \tag{23}$$

4. Results and analysis

In the previous chapter, the distributions of velocity, temperature, shear stress and Nusselt numbers on the channel walls were determined as a function of the parameters important for this considered problem. Among the influential parameters is the parameter M, which can be changed, and it also depends on the characteristic speed. In the available literature, this speed is defined in different ways, and here it is further defined in the form [8] $U_0=\nu_f/h,$ where ν_f – is the coefficient of kinematic viscosity of the base fluid. For the characteristic speed defined in this way, the parameter M becomes the Brinkmann number.

Used values of physical properties for blood and nanoparticle materials are given in Table 1 [7,21].

Table 1. Physical properties

Supstance properties	blood	Al_2O_3	TiO_2	MgO
$\rho\left(kg/m^3\right)$	997.1	3970	4250	3560
$c_p\left(J/(kgK)\right)$	4179	765,	686.2	955
$K\left(W/(Km)\right)$	0.613	40	8.9538	45
$\sigma\left(S/m\right)$	5.5x10^{-6}	35x10^{6}	2.6x10^{6}	5.392x10^{-7}
$\mu\left(Pas\right)$	0.001	-	-	-
$\beta\left[K^{-1}\right]$	0.18x10^{-5}	0.85x10^{-5}	0.90x10^{-5}	1.13x10^{-5}

The distributions of speed, temperature, shear stress and Nusselt numbers given analytically in the previous chapter depend on the type of base fluid and the type of nanoparticle material. In this section, a part of the obtained results is given for the case when the base fluid is blood, and the nanoparticles are made of aluminum oxide, magnesium oxide, and titanium dioxide. Velocity and temperature plots are given as graphs, and shear stresses and Nusselt numbers are tabulated.

Figures 2 and 3 show the graphs of the velocity distribution and temperature distribution of THNF in the channel for different values of the Ha number and the constant values of the other factors are given in these figures, respectively. It can be seen from Figure 2 that an increase in the value of the Ha number leads to an acceleration of the fluid flow in the channel and to an increase in the shear stress on the channel walls. The cause of this phenomenon is the increase in the intensity of the Lorentz force with an increase in the Ha number, which here, given the negative value of the external electrical load factor, represents the driving force. The velocity distributions are symmetrical in relation to the longitudinal axis of the channel. It can be seen from Figure 3 that an increase in the Ha number, for constant values of other factors, causes an increase in the temperature in the channel. The reason for the increase in the temperature of the fluid in the channel is the increase in Joule's heat with the increase in the Ha number.

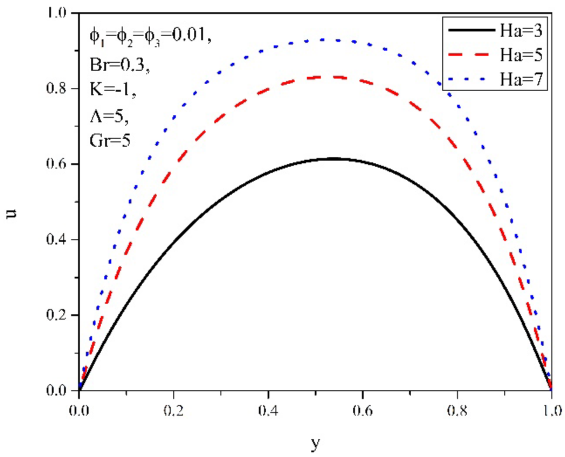

Fig. 2 Velocity distributions for different Ha values

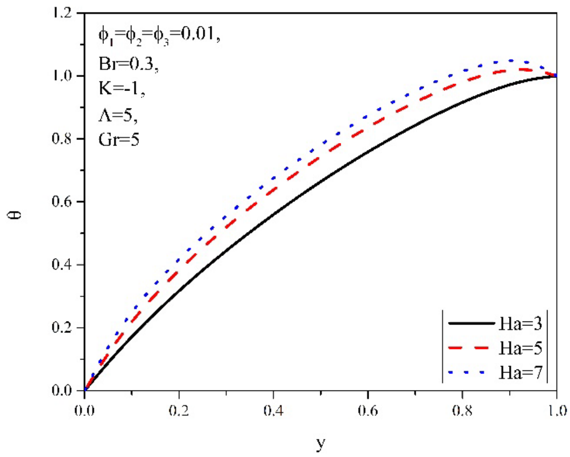

Fig. 3 Temperature distributions for different Ha values

Distributions of velocity and temperature of THNF in the channel for different values of the porosity factor, and constant values of the other factors are shown in Figures 4 and 5, respectively. It can be seen from Figure 4 that the growth of the porosity factor causes the flow in the channel to slow down. The cause of this decrease in the speed of the fluid flow is the increase in the intensity of the Darcy force with the growth of Λ, which represents the force of resistance to the flow of the fluid. As the factor Λ increases, the shear stresses on the channel walls decrease. In this case too, the speed distributions are symmetrical. It can be seen from Figure 5 that the temperature of the fluid in the channel increases with the increase in the value of Λ. The reason for this increase in temperature is the growth of Darcy dissipation with the increase of the factor Λ.

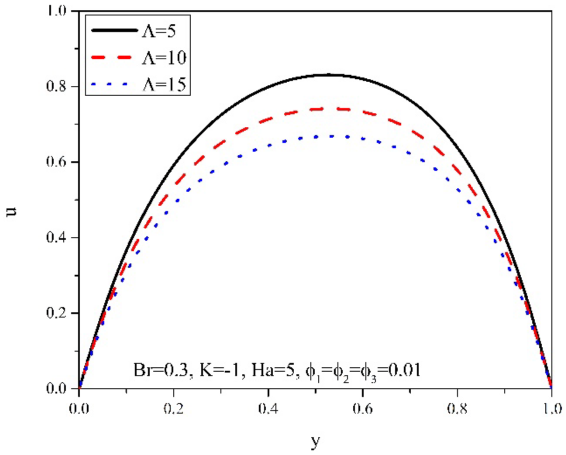

Fig. 4 Velocity distributions for different Λ values

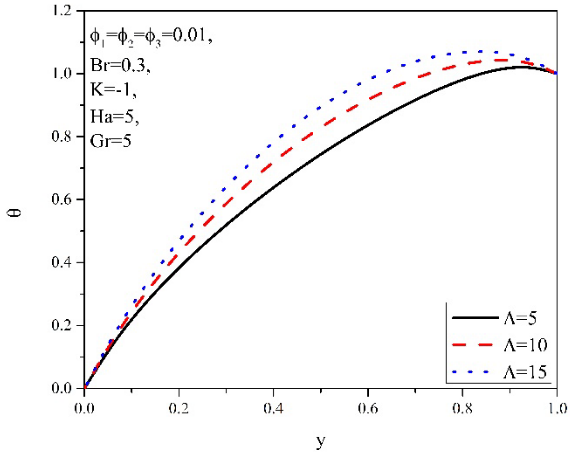

Fig. 5 Temperature distributions for different Λ values

Figures 6 and 7 show graphs of the distribution of speed and temperature for different values of the external electrical load factor K, and for constant values of the other factors given in these figures, respectively. It can be seen from Figure 6 that for K=0, the fluid flow velocity is of low intensity. For larger absolute values of K, the flow velocities are higher, and changing the sign of the factor K changes the direction of the flow velocity. The reason for this is the change in the direction of the external electric field. It can be seen from Figure 7 that the growth $|K|$ causes an increase in the temperature of the fluid in the channel. The cause of this temperature increase is the increase of Joule's heat with $|K|$ growth. For K=0, the heat transfer in the channel is mainly by conduction.

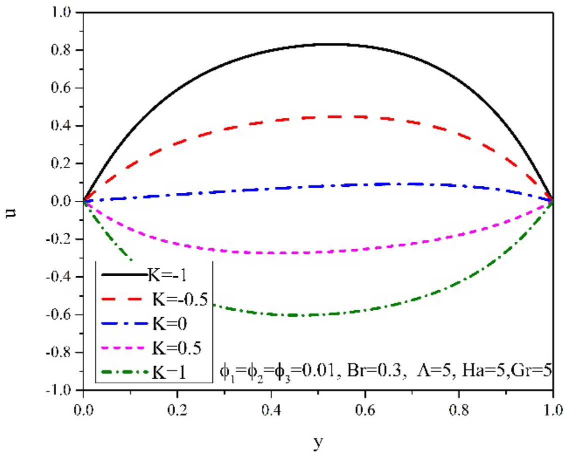

Fig. 6 Velocity distributions for different K values

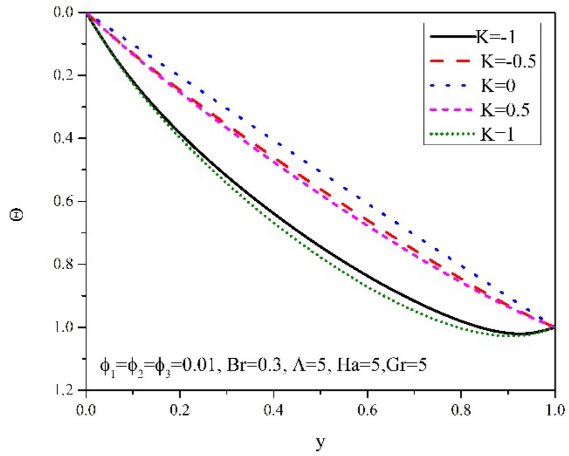

Fig. 7 Temperature distributions for different K values

Distributions of fluid velocity and temperature in the channel for different values of other factors are shown in Figures 8 and 9, respectively. It can be seen from Figure 8 that higher values of the Gr number correspond to faster fluid flows in the channel and lower shear stresses on the channel walls. The speed distribution graphs are symmetrical. The cause of this increase in flow speed is the growth of buoyancy force with increasing Gr number. As the Gr number increases, the temperature of the fluid in the channel increases, as can be seen from Figure 9. Heat transport is from the fluid to the right wall of the channel for the temperature distributions shown. This increase in the temperature of the fluid in the channel occurs because higher values of the Gr number correspond to higher speeds, and then higher amounts of Joule heat.

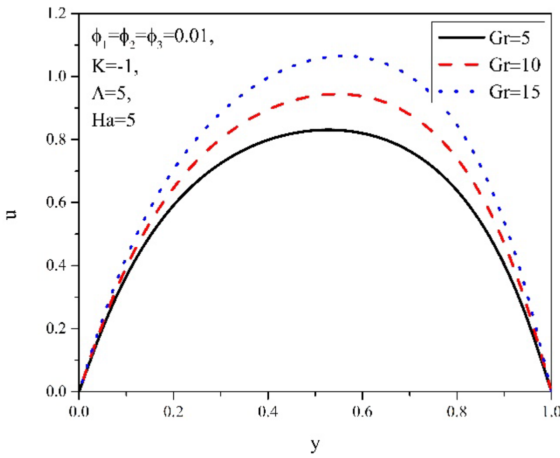

Fig. 8 Velocity distributions for different Gr values

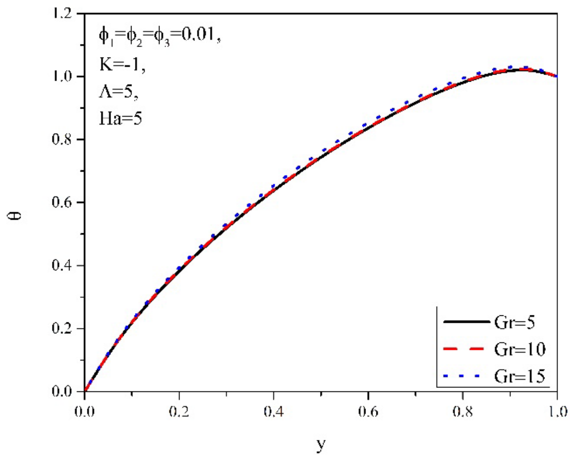

Fig. 9 Temperature distributions for different Gr values

From Figure 10, it can be seen that the flow rate is the highest for HNF, then NF, then classic fluid, and the lowest for THNF. For physical interpretation, viscous and Lorenz force relations are used. In NF, the Lorentz force is dominant in relation to the viscosity force and leads to an increase in speed in relation to the speed of a classic fluid. With HNF, the Lorentz force is even more dominant and leads to an increase in speed compared to the speed of NF. Finally, with THNF, the viscosity force is dominant compared to the Lorentz force and the velocity is the lowest. Figure 11 shows that the temperature is the highest for THNF, followed by NF and HNF, and the lowest for the classic fluid. This was brought about by the relations of viscous dissipation and Joule's heat in the flow of these fluids.

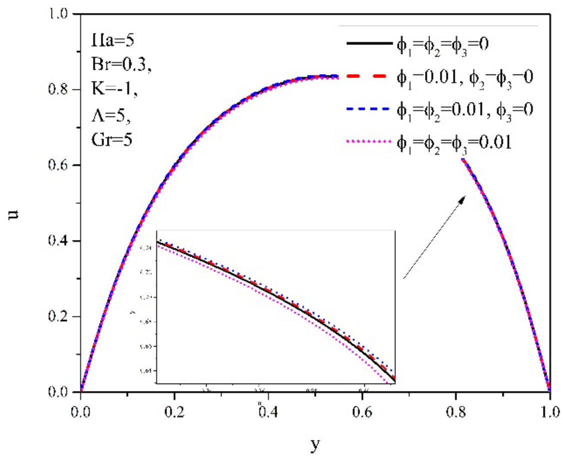

Fig. 10 Velocity distributions for different ϕ values

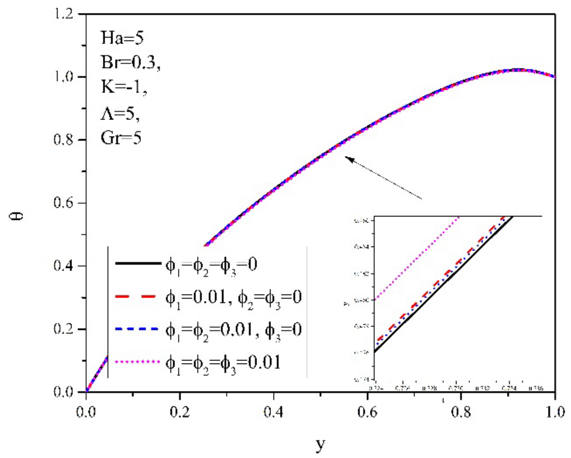

Fig. 11 Temperature distributions for different ϕ values

Table 2. Values of shear stresses and Nusselt numbers

	τ_1	τ_2	Nu_1	Nu_2
Ha=3	2.912266	-3.67165	2.081837	-0.50583
Ha=5	5.126765	-5.77732	2.952918	-1.34026
Ha=7	7.289024	-7.83983	3.733612	-2.01989
K=-1	5.126765	-5.77732	2.952918	-1.34026
K=-0.5	2.628182	-3.27957	1.563802	0.31941
K=0	0.200269	-0.85248	1.105691	1.048071
K=0.5	-2.15697	1.503931	1.578585	0.845726
K=1	-4.44355	3.789676	2.982485	-0.28762
Λ =5	5.126765	-5.77732	2.952918	-1.34026
Λ=10	4.770315	-5.39505	3.179914	-1.45368
Λ=15	4.474055	-5.07584	3.360976	-1.55508

$\phi_1 = \phi_2 = \phi_3 = 0$	4.82886	-5.41528	2.760032	-1.26556
$\phi_1 = 0.01$ $\phi_2 = \phi_3 = 0$	4.964588	-5.56803	2.838747	-1.30024
$\phi_1 = \phi_2 = 0.01$ $\phi_3 = 0$	4.966532	-5.57311	2.835411	-1.30651
$\phi_1 = \phi_2 = 0$ $\phi_3 = 0.01$	4.849357	-5.46303	2.794903	-1.26539
Gr=5	5.126765	-5.77732	2.952918	-1.34026
Gr=10	5.447907	-6.75043	2.992951	-1.96475
Gr=15	5.787437	-7.74802	3.068626	-2.65818

Table 2 gives values of shear stresses on channel walls and local values of Nusselt number on walls for parameter values $\phi_1 = \phi_2 = \phi_3 = 0.01, Br = 0.3, \Pr = 5, Ec = 2, K = -1, \Lambda = 5, Gr = 5$ (except when they change). From this table it can be seen that higher values of Ha and Gr numbers correspond to higher values of shear stresses and higher values of Nusselt number on both walls of the channel, while higher values of the porosity factor correspond to lower values of shear stress and higher values of Nusselt numbers on both walls. Higher values of $|K|$ correspond to higher values τ_1, τ_2 *and* Nu_1.

5. Conclusion

EMHD flow and THNF heat transport in a vertical channel filled with a porous medium are discussed in the paper. The channel walls are two parallel vertical plates with constant but different temperatures. Using the perturbation method, analytical distributions of fluid velocity and temperature, shear stresses and local Nusselt numbers on the walls were determined. Part of the obtained results for Al_2O_3+MgO+TiO_2/blood is given in the form of graphs for velocity and temperature distributions and in the form of tables for shear stresses and Nusselt numbers on the channel walls.

Based on the analysis of the results appropriate conclusions were drawn. It was concluded that the growth of the Hartmann number accelerates the fluid flow increases the temperature of the fluid, increases the shear stresses and Nusselt numbers on the channel walls. The growth of the porosity factor slows down the flow, increases the temperature of the fluid, reduces the stresses and increases the Nusselt numbers on the walls. Increasing K accelerates the flow and can change its direction depending on the direction of the electric field. Higher values of K correspond to higher temperatures. The influence of the Grashof number is qualitatively the same as the influence of the Hartmann number. For THNF, the speed is the lowest and the temperatures are the highest compared to these values for HNF, NF and base fluid (blood).

Acknowledgements

This research was financially supported by the Ministry of Education, Science and Technological Development of the Republic of Serbia.

References

[1] CHOI S.U.S. (1995) Enhancing thermal conductivity of fluids with nanoparticles, Developments and Applications of Non-Newtonian Flows, MD vol. 231 and FED vol. 66 ASME, pp. 95-105.
[2] LIMA J. A., ASSAD G. E. and PAVIA H. S. (2016) *A simple approach to analyze the fully developed two-phase magnetoconvection type flows in inclined parallel-plate channels*, Latin American Applied Research, 46(3), pp. 93-98, doi:10.52292/jaar.2016.333
[3] T.Linga Raju and P. Satish (2023), Slip regime MHD 2-liquid plasma heat transfer flow with Hall currents between parallel plates, Int. J. Of Applied Mechanics and Engineering, vol. 28, No. 3, pp. 65-85, doi:10.59441/ijame/172898
[4] Milica Nikodijević, Živojin Stamenković, Jelena Petrović, Miloš Kocić, (2020), Unsteady Fluid Flow and Heat Transfer Through a Porous Medium in a Inclined Magnetic Field, Transactions of Famena, Vol. 44(4), pp. 31-46, doi:10.21278/TOF.444014420
[5] YADAV P.K., KUMAR A., EL_SAPA S. AND CHAMKHA A.J. (2022) Impact of thermal radiation and oriented magnetic field on the flow of two immiscible fluids through porous media with different porosity, Waves in Random and Complex Media, doi:101080/17455030.2022.2118897
[6] [Aaiza Gul, Ilyas Khan and Sharidan Shafie (2018), Radiation and Heat generation effects in magnetohydrodynamic mixed convection flow of nanofluids, Thermal Science, Vol. 22, No. 1A, pp. 51-62, doi:10.2298/TSCI150730049G

[7] S. Das, R. N. Jana, O. D. Makinde (2015), Mixed convective magnetohydrodynamic flow in a vertical channel filled with with nanofluid, Engineering Science and Technology, an International Journal doi: 10.1016/j.jestch.2014.12.009
[8] UMAVATHI J.C., SHEREMET M.A. (2020) Heat transfer of viscous fluid in a vertical channel sandwiched between nanofluid porous zones, Journal of Thermal Analysis and Calorimetry 144(4), doi:10.1007/S10973-020-09664-1

[9] J.C. Umavathi and Ali J. Chamkha(2021) , Thermo-Solutal convection of a Nanofluid Utilizing Fourier's-Type Compass Conditions, Journal of Nanofluids 9, No. 4, pp. 362-374, doi:10.1166/jon.2020.1759
[10] [J.C.Umavathi and Hakan F.Oztop (2021), Investigation of MHD and applied electric field effects in a conduit cramed with nanofluids, International Communications in Heat and Mass Transfer, Vol. 121:105097, doi:10.1016/j.icheatmasstransfer.2020.105097
[11] PETROVIĆ J.D., STAMENKOVIĆ Ž., BOGDANOVIĆ JOVANOVIĆ J:, NIKODIJEVIĆ M., KOCIĆ M., NIKODIJEVIĆ D. (2022) *Electro-Magneto Convection Immiscible Pure Fluid and Nanofluid*, Transactions of FAMENA 46(3):13-28, doi:10.21278/TOF.463036021
[12] Jelena D. Petrović, Živojin Stamenković, Miloš Kocić, Milica Nikodijević, Jasmina Bogdanović Jovanović, Dragiša D. Nikodijević (2022), Magnetohydrodynamicflow and mixed convection of a viscous fluid and a nanofluid a porous medium in a vertical channel, Thermal Science Volume 27, Issue 2 Part B, pp. 1453-1463, doi:10.2298/TSCI220903188P
[13] Petrović D. Jelena, Nikodijević Đorđević Milica, Kocić Miloš, (2023), Electromagnetic hydrodynamic flow and heat transfer of a Casson nanofluid Fe_3O_4-blood in a porous medium, Thermal Science Volume 27, Issue 6 Part A, pp. 4461-4472, doi:10.2298/TSCI230516169P
[14] M.Padma Devi, Kamal Goyal, S. Srinivas, B. Satyanarayana (2024), Effects of different nanoparticles on the two immiscible liquids flow in an inclined channel with Joule heating and viscous dissipation, Gulf Journal of Mathematics Vol. 16, Issue 2, 278-290, doi:10.56947/gjam.V16i2.1815
[15] Radma Devi Medisetty, Srinivas Suripeddi, Satyanarayana Badeti, Vajraveln Kuppalapalle (2024), Pulsatile MHD flow of two immiscible nanofluids through a porous channel with slip effects, Int. J. Of Applied Mechanics and Engineering, vol. 29, No. 1, pp. 105-129, doi:10.59441/ijame/175745
[16] Hang Xu and Qiang Sun, (2019), Generalized Hybrid Nanofluid with the Application of Fully Developed Mixed Convection Flow in a Vertical Microchannel, Communications in theoretical Physics, Vol. 71, No. 8, 903-911, doi:10.1088/0253-6102/71/8/903
[17] Ali J. Chamkha, A.S. Dogonchi and D.D. Ganji, (2019), Magneto-hydrodinamic flow and heat transfer of a hybrid nanofluid in a rotating system among two surfaces in the presence of thermal radiation and Joule heating, AIP Advances 9, 025103, doi:10.1063/1.5086247
[18] M.V.V.N.L.Sudharami, D.G. Prakasha, K.Ganesh Kumar and Ali J.Chamkha (2023), Computational assessment of hybrid and try hibrid nanofluid influenced by slip flow and linear radiation, Eur. Phys. J. Plus 138, 257, doi:10.1140/epjp/S13360-023-03852-2
[19] Ebrahem A. Algehyne, Haiffa F. Alrihieli, Muhammad Bilal, Anwar Saeed and Wajaree Weera (2022), Numerical Approach toward Ternary Hybrid Nanofluid Flow Using Variable Diffusion and Non-Fouriers Concept, ACS Omega 7 (33), 29380-29390, doi:10.1021/acsomega.2c03634
[20] Saman Riaz, Muhammad F.Afzaal, Zhan Wang, Ahmed Jan and Umer Farooq (2023), Numerical heat transfer of non-similar ternary hybrid nanofluid flow over lineary stretching surface, Numerical Heat Transfer, Part A: Applications, doi:10.1080/10407782.2023.2251093
[21] A. Manigandan, Panyam Vankata Satya Narayana, (2024), Impact of variable fluid characteristics on MHD hybrid nanofluid ($MgO+ZnO/H_2O$) flow over an exponentially elongated sheet with non uniform heat generation, Case Studies in Thermal Engineering 55 (2024) 104077, doi:10.1016/j.csite.2024.104077